Effect of Temperature on the Evolution of Physical Structure and Chemical Properties of Bio-char Derived from Co-pyrolysis of Lignin with High-Density Polyethylene

Weimin Chen, Shukai Shi, Thiphuong Nguyen, Minzhi Chen, and Xiaoyan Zhou *

Bio-chars were produced by co-pyrolysis of lignin with high-density polyethylene at 350 °C, 450 °C, and 550 °C. X-ray diffraction (XRD), Raman spectroscopy, automated surface area and pore size analysis, scanning electron microscopy (SEM), Fourier transform infrared (FT-IR) spectroscopy, X-ray photoelectron spectroscopy (XPS), and electron spin resonance (ESR) spectroscopy were performed on bio-char to reveal the effect of temperature on its physical structure and chemical properties. All of the bio-chars demonstrated a highly disordered, turbostratic structure and exhibited a wide pore distribution. Dramatic losses of carbonyl, hydroxyl, and C-H groups indicated the development of condensed aromatic structure in the bio-chars. Specifically, biochar produced at 450 °C showed the highest degree of aromaticity, which is the relative content of aromatic structure with small fused rings and free radical concentration. This structure has more potential application in composite production and as solid fuel for its combustion or gasification. Moreover, biochar produced at 550 °C had the greatest porosity development, favoring its use as a precursor for activated carbon production.

Keywords: Co-pyrolysis; Lignin; High-density polyethylene; Aromatic structure; Chemical property

*Contact information: College of Materials Science and Engineering, Nanjing Forestry University, Nanjing 210037, China; *Corresponding author: zhouxiaoyan@njfu.edu.cn*

INTRODUCTION

Lignin is the second most abundant natural polymer after cellulose, and it is the main byproduct of the pulp and paper industry (Kong *et al.* 2009). Its massive annual production worldwide yield reaches 50 million metric tons. However, lignin is usually considered as an energy source, with low-added value (Pinto *et al.* 2015). Only a minor portion of the available lignin is utilized by traditional management processes, such as burning as low-valued fuels, which cannot fundamentally solve the environmental and clean-energy recycling issues. The massive production of plastic as a municipal solid waste (MSW) has reached almost 20 million tons in China. Moreover, most plastic species cannot be naturally degraded, which has prompted an increased interest in thermal conversion, such as pyrolysis, which can convert feedstocks into clean fuels and recover chemicals (Ucar *et al.* 2014; Veksha *et al.* 2014).

Co-pyrolysis has been applied to produce bio-fuels in recent years, especially bio-gas and bio-oil (Suelves *et al.* 2002; Martinez *et al.* 2014). Plastic with higher hydrogen content could be used as a hydrogen donor in co-pyrolysis with biomass or coal of less

hydrogen content, which could balance the carbon, oxygen, and hydrogen in the feedstock. This process could result in a strong upgrading effect on its derived product, such as bio-oil and bio-char (Shadangi and Mohanty 2015). Previous studies have demonstrated that co-pyrolysis of biomass with plastic results in an increase in bio-oil yield and an improvement in bio-oil quality (Onal *et al.* 2014). Moreover, co-pyrolysis of biomass with plastic could solve the problem with different components of MSW that are not easily separated from the post-consumer stream.

However, little work has focused on bio-char derived from co-pyrolysis. It has been demonstrated that bio-char obtained by co-pyrolysis of biomass with high-density polyethylene is upgraded, with the characteristics of lower oxygen-containing groups, increased aromatic structure, higher calorific value, and greater porosity development compared with biomass pyrolyzed alone (Chen *et al.* 2015).

Almost all carbonaceous biomass can be converted to bio-char using slow or fast pyrolysis. Bio-char can be used as a fuel cell catalyst for biomass gasification and/or applied in the field of catalyst support for tar cracking because of its pore texture (Sutton *et al.* 2001). The aromatic structure and large carbon content of bio-char favors its application as a precursor for activated carbon and supercapacitor production (Peng *et al.* 2013). Bio-char also can be used in composite materials, mostly as filler in polymer-biochar composites (Ahmetli *et al.* 2004). In addition, the surface chemical property and condensed aromatic structure in bio-char improves soil by enhancing soil fertility, soil microbial activity, and nutrient availability (Bornermann *et al.* 2007; Steinbeiss and Gleixner 2009). Because of its relatively low oxygen content, bio-char can be directly used in carbon fuel cells with a composite electrolyte of samarium-doped ceria and a eutectic carbonate phase (Yu *et al.* 2014).

In this study, lignin was selected as a bio-char precursor because of its high carbon content, aromatic structure, and abundant availability. High-density polyethylene was used as a hydrogen donor for co-pyrolysis. Co-pyrolysis derived bio-chars were produced at 350 °C, 450 °C, and 550 °C. X-ray diffraction and Raman spectroscopy were used to investigate crystalline and aromatic structural changes. The pore texture of co-pyrolysis-derived bio-char was revealed using an automated surface area and pore size analyzer and was confirmed by scanning electron microscopy. Fourier transform infrared spectroscopy and X-ray photoelectron spectroscopy analysis were performed to investigate the surface atomic components and chemical functional group changes. The chemical activity of bio-char was studied using electron spin resonance analysis.

EXPERIMENTAL

Materials

Lignin was obtained from pulping black liquor (PBL), which was purchased from a local paper mill (Yonghong, Nanjing, China). The separation and purification of lignin from PBL was performed as described (Zhang *et al.* 2011). High-density polyethylene (HDPE) was obtained from shampoo bottles. Lignin and HDPE were ground by a grinder and then sieved to a particle size of less than 1 mm using mesh screen. Lignin and HDPE powders were mixed in a 50:50 (w/w) ratio and rolled for 12 h, then dried at 103 °C for 8 h for further carbonization.

Methods

Bio-char preparation

The co-pyrolysis reactor was previously described (Chen *et al*. 2015). It was operated under a 20 mL/min N_2 flow with high purity (99.99%). Vacuum pump was used before each experiment started to ensure pure N_2 atmosphere in the quartz tube. Approximately 6 g of mixed feedstock (lignin/HDPE weight ratio of 50:50) was placed in crucible for each experiment and heated up to a final pyrolysis temperature of 350 °C, 450 °C, or 550 °C at a heating rate of 10 °C/min and then incubated at the given temperature for 60 min. The co-pyrolysis derived bio-chars produced at 350 °C, 450 °C, or 550 °C were obtained from the crucible after pyrolysis was finished and were denoted as CB-350, CB-450, and CB-550, respectively.

Bio-char characterization

The crystalline structure of bio-char was analyzed using an Ultima-IV X-ray diffractor (Rigaku Corporation, Tokyo, Japan). The 2θ value for all samples was recorded from 5 ° to 65 °, with a step size of 0.02 °/s using Cu Kα radiation (40 kV, 200 mA).

The amorphous, crystalline, and aromatic nature of the bio-char samples was investigated using Raman spectroscopy with a DXR532 apparatus (Nicolet, Michigan, USA) under laser radiation operating at a wavelength of 532 nm, a spectral resolution of 4 cm^{-1}, laser power of 10%, exposure time of 10 s, and a total of 30 acquisitions. The Raman spectra were collected between 800 and 1800 cm^{-1} and fitted using XPSPEAK Software (Version 4.1, Freeware Co., Hongkong, China).

The Brunauer-Emmett-Teller (BET) surface area and pore distribution were studied using an automated surface area and pore size analyzer (Micromeritics Co., Norcross, GA, USA). The N_2 adsorption isotherms were obtained at 77 K. The BET surface area for all samples was obtained using the BET standard method (Mushrif *et al.* 2008). Total pore volume was calculated by converting the amount of nitrogen gas adsorbed at a relative pressure of 0.99 to the volume of liquid adsorbed. Micropore volume was calculated using the *t*-plot method (Mushrif *et al.* 2008).

Surface morphology was investigated using scanning electron microscopy (SEM; Quanta 200, FEI Co., Hillsboro, OR, USA). Five kV voltage and high vacuum mode were used for all tests. All samples were gold-coated using a PECS coating machine (Gatan Inc., Pleasanton, CA, USA) to reduce the charging effects.

Chemical functional groups were analyzed using Fourier transform infrared (FT-IR) spectroscopy, performed in a NEXUS 870 (Nicolet Instrument Corp., Madison, WI, USA). One percent of the bio-char samples were carried using KBr discs. All samples were scanned and recorded in the wave number range from 400 to 4000 cm^{-1}, with a resolution of 4 cm^{-1}. The precision was no more than 0.01 cm^{-1}.

Surface elemental composition and chemical functional groups were examined using X-ray photoelectron spectroscopy (XPS) in an AXIS Ultra DLD (Shimadzu, Tokyo, Japan). Survey scanning was performed for low-resolution spectra in the binding energy region from 0 to 1100 eV, and the C1s scan of high-resolution spectra from 277 to 396 eV were recorded with a pass energy of 10 eV and non-monochromatic Mg Kα and Al Kα X-radiations ($h\gamma$ = 1253.7 eV and 1486.7 eV, respectively). The C1s spectra were deconvoluted into five components using XPSPEAK Software.

Chemical activity was analyzed using electron spin resonance (ESR) spectrometry (EMX-10/12, Bruker Corp., Hannover, Germany), operating at a microwave frequency of

9.8617GHz. Bio-char samples were placed in 4-mm borosilicate tubes and examined at room temperature during a scan time period of 4 min and a time constant of 0.25 s.

RESULTS AND DISCUSSION

X-Ray Diffraction Analysis

X-ray diffraction was applied to study the short-range ordered structures and crystalline structures of bio-char samples (Liao *et al.* 2007) (Fig. 1). Peaks at approximately 23°, corresponding to the 002 plane reflection of graphite crystallite, were observed in all samples, implying that graphite-like structures were present in the bio-char. Furthermore, the broader width and shifted position of this peak compared with pure graphite indicated the highly disordered and turbostratic character of the bio-char structure. Moreover, the intensity of this peak decreased as the pyrolysis temperature increased, indicating that the bio-char structure was damaged at higher pyrolysis temperatures. Several new peaks appeared in CB-550, showing the presence of several minerals (Fan *et al.* 2015). This result implied that pyrolysis at higher temperatures results in higher ash content.

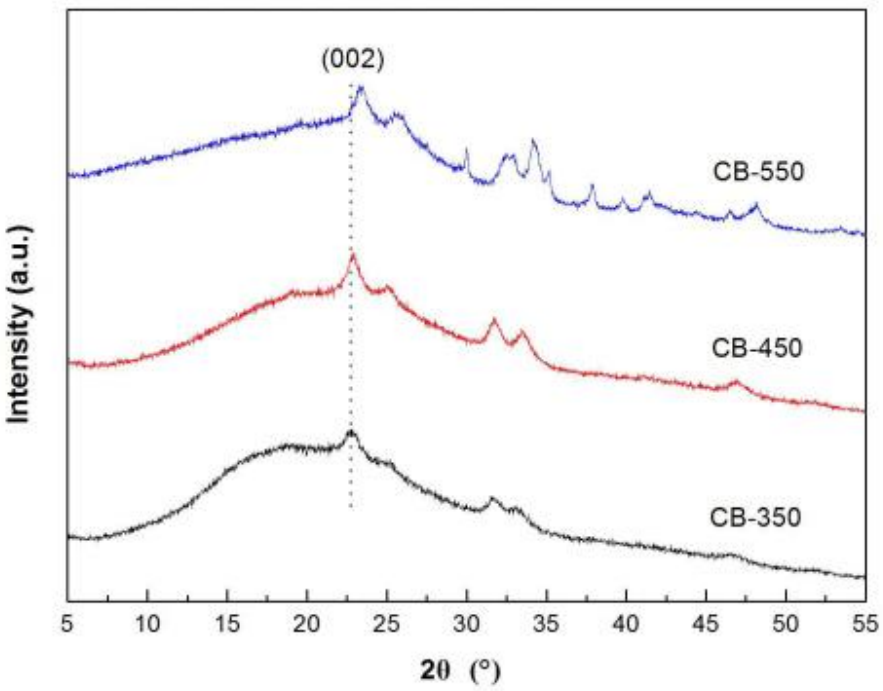

Fig. 1. X-ray diffraction of bio-char samples

Raman Spectroscopy

Raman spectroscopy was applied to investigate structure, specifically the amorphous, crystalline, and aromatic nature of co-pyrolysis-derived bio-char (Keown *et al.* 2007). Figure 2a shows the Raman spectrum of lignin and its derived bio-char samples. The band intensity initially decreased as the pyrolysis temperature increased, which was related to the loss of oxygen-containing groups in the bio-char structure, resulting in a decline in the Raman scattering ability. An obvious increase in the band intensity of CB-

550 was observed. This result was attributed to the high relative content of minerals (confirmed by XRD analysis), especially Ca and Na, which passively impact the Raman peak intensity by accelerating the formation of condensed aromatic ring structures (Keown *et al.* 2007). Moreover, two broad peaks at 1340 cm^{-1} and 1580 cm^{-1} were observed, implying structural disorder and multiphase bio-char structure. The Raman spectra of those bio-char samples were fitted into 9 Gaussian bands from 800 cm^{-1} to 2000 cm^{-1} (Guo *et al.* 2008; Zhang *et al.* 2011) (Fig. 2b). Only 5 bands (D, V_R, V_L, G, and G_R) were predominant, representing the typical aromatic structures of those bio-chars. The band at 1590 cm^{-1} (G-band) was attributed to aromatic ring quadrant breathing (Li *et al.* 2006). The D band at 1300 cm^{-1} referred to structures with more fused aromatic rings (≥ 6 rings) (Zhang *et al.* 2011), while the V_R, V_L, and G_R bands at 1380 cm^{-1}, 1460 cm^{-1}, and 1540 cm^{-1}, respectively, corresponded to the amorphous structure with smaller fused rings (3 to 5 fused aromatic rings) (Kim *et al.* 2011 and Guo *et al.* 2008).

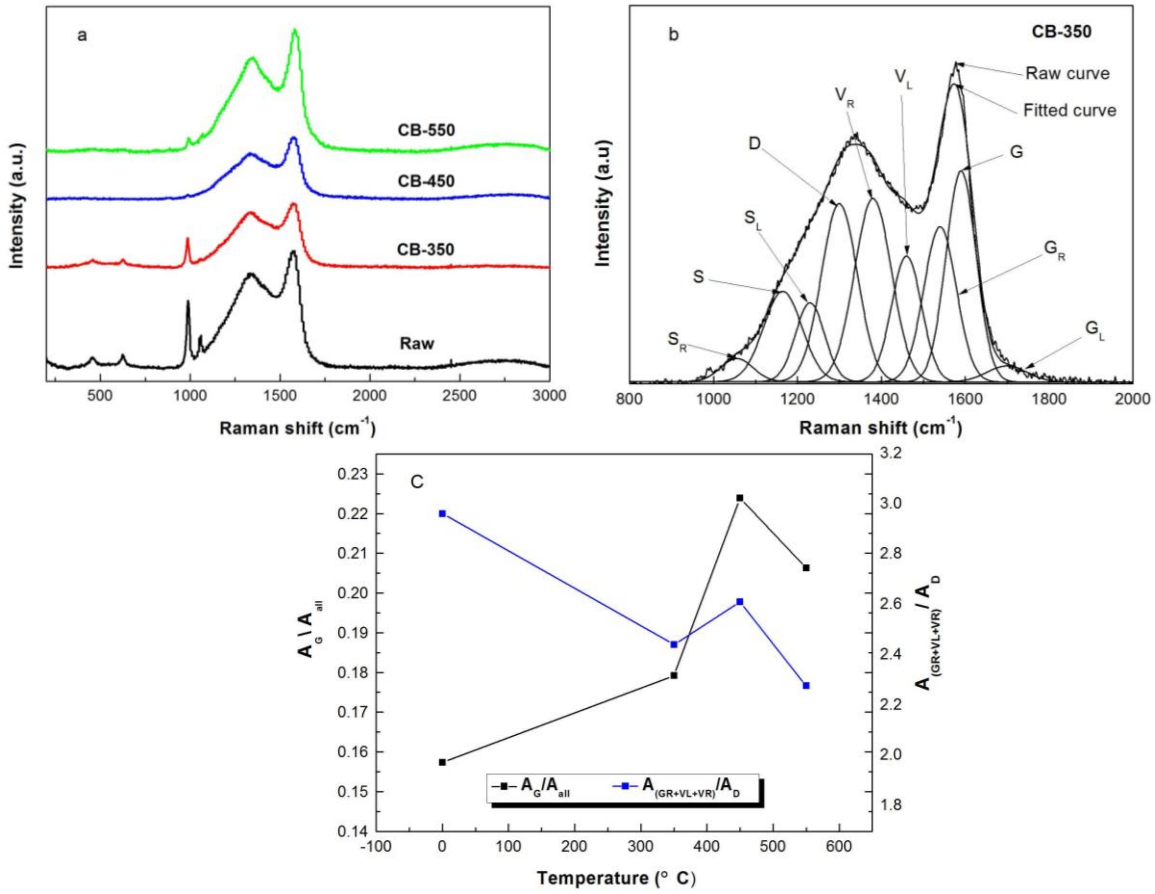

Fig. 2. (a) Raman spectrum of lignin and its derived bio-char samples; (b) deconvolution for Raman spectrum of CB-350; (c) A_G/A_{all} and $A_{(VR+VL+GR)}/A_D$ of lignin and its derived bio-char samples

The band area ratio (A_G/A_{all}) between the G-band and all 9 bands (S_R, S, S_L, D, V_R, V_L, G, G_R, and G_L) was calculated to reflect the evolution of aromaticity in the bio-char samples (Liu *et al.* 2012). As illustrated in Fig. 2c, the A_G/A_{all} value initially increased and reached the maximum at 450 °C. This result was attributed to the condensation of

aromatic structures and the removal of oxygen-containing groups present in the crosslinking of carbon, yielding non-graphitizing carbon. An obvious decrease in A_G/A_{all} was observed at 550 °C. This result was related to the opening of the benzene ring, beginning the conversion of benzene to a linear C-C chain.

The band area ratio ($A_{(VR+VL+GR)}/A_D$) between the sum of the VR, VL, and GR bands and the D band was used to compare the aromatic content containing small fused rings *vs*. more fused rings (Guo *et al.* 2008). This value was also used to evaluate the bio-char reactivity (McDonald-Wharry *et al*. 2013). The $A_{(VR+VL+GR)}/A_D$ value of the bio-chars showed similar variation trends to A_G/A_{all} and reached a maximum at 450 °C. According to Liu *et al.* (2008), the mass loss rate peak of lignin appears at 450 °C, indicating a strong volatile char interaction on the bio-char surface that favors the accumulation of small aromatic-fused rings. It should be noted that bio-char samples with a higher content of small aromatic-fused rings exhibited higher reactivity, favoring its combustion or gasification as solid fuel (McDonald-Wharry *et al.* 2013).

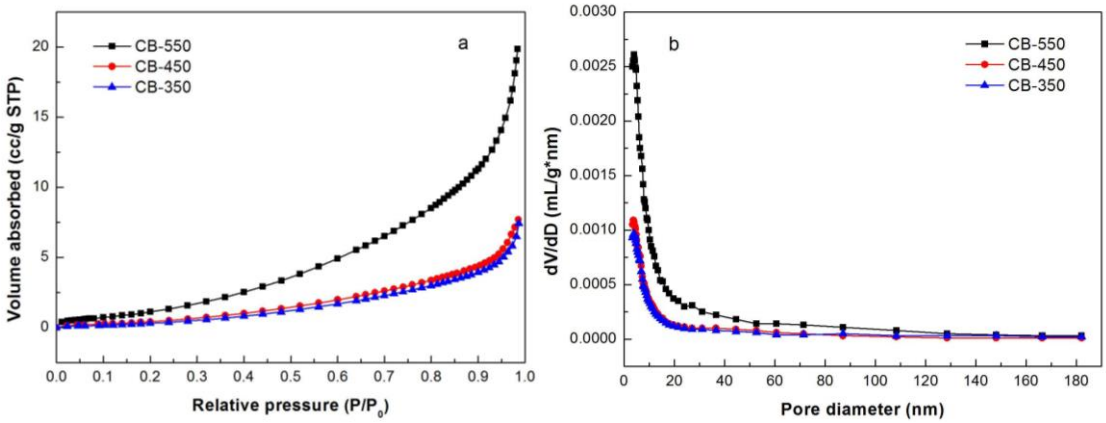

Fig. 3. (a) N_2 adsorption isotherms of co-pyrolysis derived bio-char at 77 K; (b) BJH pore distribution of co-pyrolysis derived bio-char

Pore Texture Analysis

The N_2 adsorption isotherms and pore size distributions of co-pyrolysis-derived bio-char samples are shown in Fig. 3. Bio-char samples demonstrated type IV isotherm curves, according to the BDDT classification system. A slight increase in adsorption volume initially appeared in the low relative pressure region, and a sharp increase was observed in the relative pressure region of 0.9 to 1.0, indicating a low level of microporosity in all samples (Mohan *et al.* 2014). Moreover, there was a gradual increase in absorption volume from 0.2 to 0.8 relative pressure, implying the presence of mesopores with a broad distribution (Mohan *et al.* 2014; Wang *et al.* 2014). As shown in Fig. 3b, pores in both bio-char samples demonstrated incomplete distribution near the lowest pore size limit, revealing the existence of micropores. Rapidly decreasing slopes were observed for all samples, and no peaks appeared at the entire pore diameter region, indicating the broad pore diameter distribution in the bio-char structure (Li *et al.* 2010). Thus, CB-550 exhibited greater porosity development than CB-450 and CB-350.

The BET surface area and pore properties of co-pyrolysis-derived bio-char samples are presented in Table 1. This data showed that pyrolysis at higher temperatures resulted in higher bio-char BET surface area, which was attributed to more volatile matter

generated, leading to the formation of more pores. Moreover, CB-550 exhibited lower average pore width compared with CB-450 and CB350. This effect was related to the shrinking effect at higher temperatures, leading to the collapse of some macropores.

Table 1. BET Surface Area and Pore Properties of Bio-Chars

Sample	BET Surface Area (m^2/g)	Total Pore Volume (cm^3/g)	Average Pore Width[a] (nm)	Micropore Volume[b] (cm^3/g)
CB-350	1.865	0.0114	24.45	0.0025
CB-450	4.318	0.0239	22.16	0.0042
CB-550	11.528	0.0496	17.21	0.0092

[a]Calculated from BET surface area and total pore volume
[b]Calculated by the *t*-plot method
Note: All data in Table 1 were calculated from adsorption isotherms

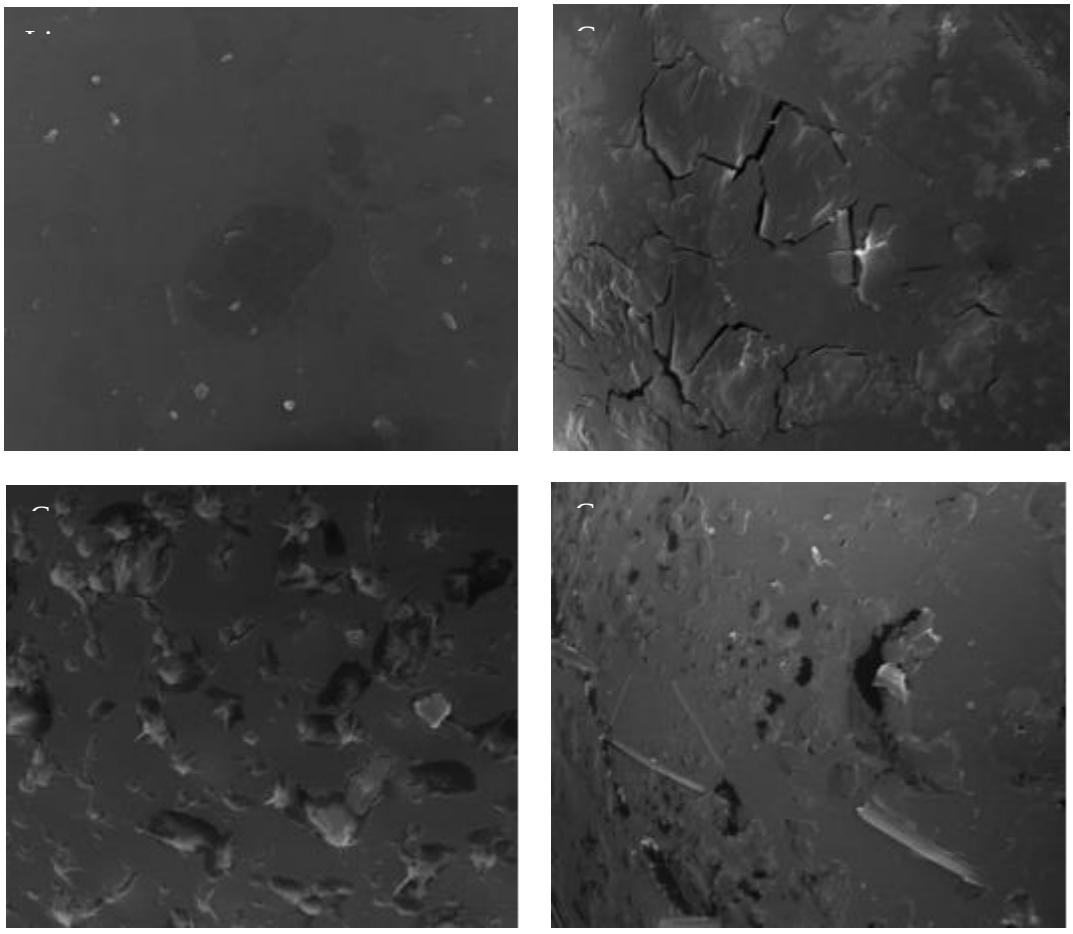

Fig. 4. Scanning electron microscopy of bio-char samples

SEM Analysis

Micrographs of co-pyrolysis-derived bio-char samples are presented in Fig. 4. Several cracks appeared on the surface of CB-350, which was attributed to the devolatilization of lignin structure with poor thermal stability. Pores with non-uniform size were observed in CB-450 and CB-550 because of the release of micromolecules

from the lignin structure. Notably, the CB-550 pores were much smaller than those in CB-450. This result may be related to pore collapse caused by higher temperatures, which was confirmed in the pore distribution analysis.

FT-IR Analysis

The FT-IR spectra of lignin and its derived bio-char samples are presented in Fig. 5. As the pyrolysis temperature increased, the adsorption intensity at 3417 cm^{-1} decreased, which was assigned to OH groups in aromatic and aliphatic structures. This result was related to breaking hydrogen bonds, which released of alcohol and water. The adsorption peak at 2935 cm^{-1} and 1035 cm^{-1} corresponded to C-H in aliphatic and aromatic structure (Sharma *et al.* 2002); these peaks were greatly decreased after pyrolysis. The peak intensity of the adsorption bands at 1597 cm^{-1}, 1265 cm^{-1}, and 1210 cm^{-1} were attributed to C=O and C-O, respectively (Elmay *et al.* 2015) and were considerably decreased at 550 °C. Consequently, pyrolysis at 550 °C resulted in a dramatic loss in carbonyl, hydroxyl, and C-H groups, indicating the significant development of aromatic structures.

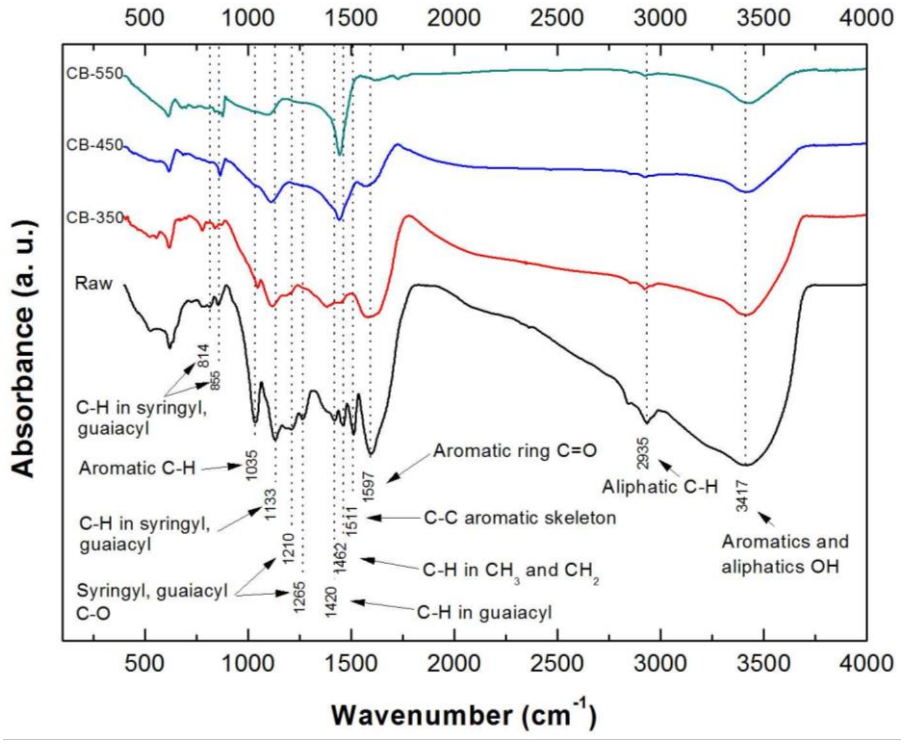

Fig. 5. FT-IR spectra of lignin and its derived bio-char samples

XPS Analysis

X-ray photoelectron spectroscopy was applied to study surface chemistry and to identify and quantify the basic elements (except hydrogen and helium) and functional groups (Sun *et al.* 2012) (Fig. 6; Table 2). As illustrated in Table 2, the O/C mass ratio decreased as the pyrolysis temperature increased, indicating the gradual development of condensed aromatic structures.

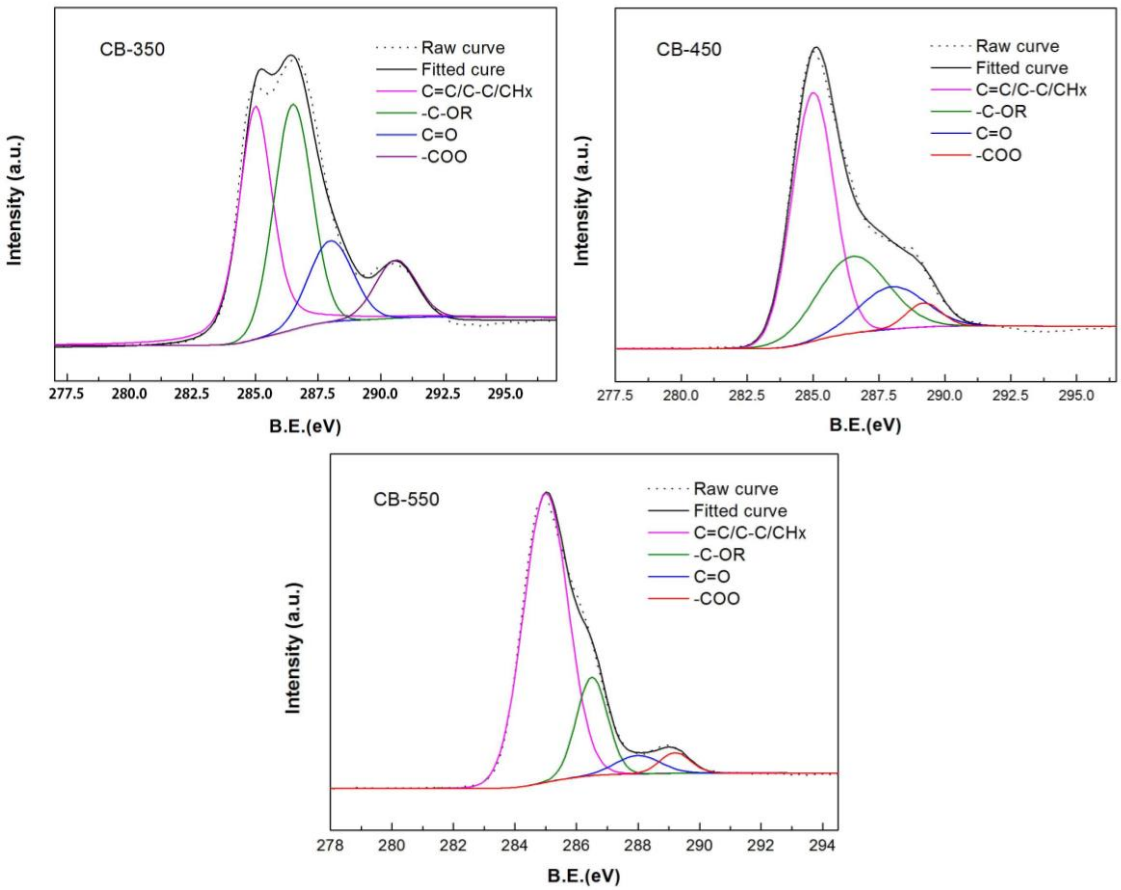

Fig. 6. Deconvolution of C1s spectra of co-pyrolysis-derived bio-char samples

Table 2. Atomic Element Composition and C1s Chemical Composition of Co-pyrolysis-Derived Bio-char Samples

Atomic Composition (%)	Bio-char Samples		
	CB-350	CB-450	CB-550
C	63.29	70.33	73.51
O	36.47	29.64	26.49
N	0.24	0.02	-
O/C	0.58	0.42	0.36
C1s composition (%)			
C=C/C-C/CHx	39.8	54.1	74.2
-C-OR	35.5	27.5	17.5
C=O	14.8	14.1	4.6
-COO	0	4.3	3.7
-O-CO-O-	9.9	-	-

According to Azargohar *et al.* (2014), the C1s spectra of the bio-char samples were deconvoluted into 5 Gaussian peaks corresponding to 5 carbon-related functional groups, namely C=C/C-C/CHx for aromatic/aliphatic carbon at 285 eV, -C-OR for ether and hydroxyl/phenol groups at 285 eV, C=O for ketone and quinone at 288 eV, -COO for carboxyl and ester at 289.2 eV, and -O-CO-O- for carbonate at 290.7 eV. C=C/C-C/CHx was the most dominant component of all samples, and it dramatically increased as the pyrolysis temperature increased. This increase was accompanied by a notable decrease in oxygen-containing groups (except COO), which agreed with the FT-IR analysis. These results were attributed to the removal of heteroatoms and aliphatic compounds during crosslinking, implying a considerable development of condensed polyaromatic skeletons in co-pyrolysis-derived bio-char and the carbon conversion into easy-graphitizing type, which was confirmed by Raman analysis. Thus, carbon enrichment in bio-char at higher pyrolysis temperatures favors its application as a precursor for activated carbon production.

ESR Analysis

Free radical formation is a significant step in bio-char evolution. Higher free radical concentration favors chemical activity (Liao *et al.* 2014). For example, radical centers in a substrate initiate the grafting of other polymers into a composite. In addition, radicals that form in the co-pyrolysis-derived bio-char favor crosslinking reactions, which enhance the physical and mechanical properties of composites (Zhou *et al.* 2013).

The *g* factor parameter identifies the type of free radical. The *g* factor and free radical concentration of lignin and co-pyrolysis-derived bio-char are presented in Table 3. A *g* factor greater than 2.0040 corresponds to oxygen-centered radicals, while a *g* factor less than 2.0030 represents carbon-centered radicals (aromatics). A *g* factor of 2.0030 to 2.0040 is attributed to mixed carbon- and oxygen-centered radicals (Di *et al.* 2006). The *g* factor decreased with increasing pyrolysis temperature to a minimum (2.0032) at 550 °C, indicating the conversion of free radicals from oxygen-centered radicals into a combination of carbon- and oxygen-centered radicals. A decrease in the *g* factor was related to the decomposition of oxygen-centered radicals with less thermal stability.

Radical concentration initially increased to a maximum at 450 °C, which reflected the breakdown of side chains and carbon-oxygen bonds in bio-char, as confirmed by FT-IR and XPS analysis. The radical concentration then decreased. Interactions between the free radicals generated from micromolecule structures at higher temperature may have been responsible for the decrease in radical concentration. It should be noted that higher free radical concentrations lead to higher chemical activity in bio-char.

Table 3. The *g* Factor and Free Radical Concentration of Lignin and Co-Pyrolysis-Derived Bio-Char Samples

	Biochar Samples			
	Raw	CB-350	CB-450	CB-550
g factor	2.0040	2.0040	2.0038	2.0032
Free Radical Concentration (spins/*g*)	3.0×10^{17}	6.96×10^{17}	1.28×10^{18}	7.0×10^{17}

CONCLUSIONS

1. All bio-chars showed a high degree of disorder, turbostratic structure, and wide pore distribution.
2. The removal of oxygen-containing groups and increased carbon density resulted in the development of condensed aromatic structures.
3. Bio-char produced at 450 °C demonstrated the highest degree of aromaticity, relative content of aromatic structure with small, fused rings, and free radical concentration. This product has potential application in composite production and as solid fuel for its combustion or gasification.
4. Bio-char produced at 550 °C exhibited the greatest porosity development and highest carbon enrichment, favoring its use as a precursor for activated carbon production.

ACKNOWLEDGMENTS

The authors are grateful for support from the Doctorate Fellowship Foundation of Nanjing Forestry University, the National Natural Science Foundation of China (Grant No. 31400515), the National Natural Science Foundation of China (Grant No.31270606), and the Priority Academic Program Development of Jiangsu Higher Education Institutions (PAPD). This paper was sponsored by the Qing Lan Project.

REFERENCES CITED

Ahmetli, G., Kocaman, S., Ozaytekin, I., and Bozkurt, P. (2004). "Epoxy composites based on inexpensive char filler obtained from plastic waste and natural resources," *Polymer Composites* 34(4), 500-509. DOI: 10.1002/pc.22452

Azargohar, R., Nanda, S., Kozinski, J. A., Dalai, A. K., and Sutarto, R. (2014). "Effects of temperature on the physicochemical characteristics of fast pyrolysis bio-chars derived from Canadian waste biomass," *Fuel* 125, 90-100. DOI: 10.1016/j.fuel.2014.01.083

Bornermann, L. C., Kookana, R. S., and Welp, G. (2007). "Differential sorption behaviour of aromatic hydrocarbons on charcoals prepared at different temperatures from grass and wood," *Chemosphere* 67(5), 1033-1042. DOI: 10.1016/j.chemosphere.2006.10.052

Chen, W. M., Chen, M. Z. and Zhou, X. Y. (2015). "Characterization of biochar obtained by co-pyrolysis of waste newspaper with high-density polyethylene," *BioResources* 10(4), 8253-8267. DOI: 10.15376/biores.10.4.8253-8267

Di, V. C., Neyman, K. M., Risse, T., Sterrer, M., Fischbach, E., Freund, H. J., Nasluzov, V. A., Pacchioni, G., and Rosch, N. (2006). "Density-functional model cluster studies of EPR g tensors of F-s(+) centers on the surface of MgO," *The Journal of Chemical Physics* 124(4), 0044708. DOI: 10.1063/1.2161190

Elmay, Y., Le Brech, Y., Delmotte, L., Dufour, A., Brosse, N., and Gadiou, R. (2015). "Characterization of *Miscanthus* pyrolysis by DRIFTs, UV Raman spectroscopy and

mass spectrometry," *Journal of Analytical and Applied Pyrolysis* 113, 402-411. DOI: 10.1016/j.jaap.2015.03.004

Fan, C., Yan, J. W., Huang, Y. R., Han, X. X., and Jiang, X. M. (2015). "XRD and TG-FTIR study of the effect of mineral matrix on the pyrolysis and combustion of organic matter in shale char," *Fuel* 139, 502-510. DOI: 10.1016/j.fuel.2014.09.021

Guo, X., Tay, H. L., Zhang, S., and Li, C. Z. (2008). "Changes in char structure during the gasification of a Victorian brown coal in steam and oxygen at 800 degrees C," *Energy & Fuels* 22, 4034-4038. DOI: 10.1021/ef800528c

Keown, D. M., Li, X. J., Hayashi, J. I., and Li, C. Z. (2007). "Characterization of the structural features of char from the pyrolysis of cane trash using Fourier transform-Raman spectroscopy," *Energy & Fuels* 21(3), 1816-1821. DOI: 10.1021/ef070049r

Kim, P., Johnson, A., Edmunds, C. W., Radosevich, M., Vogt, F., Rials, T. G., and Labbe, N. (2011). "Surface functionality and carbon structures in lignocellulosic-derived biochars produced by fast pyrolysis," *Energy & Fuels* 25(10), 4693-4703. DOI: 10.1021/ef200915s

Kong, F. J., Parhiala, K., Wang, S. J., and Fatehi, P. (2009). "Preparation of cationic softwood kraft lignin and its application in dye removal," *European Polymer Journal* 67, 335-345. DOI: 10.1016/j.eurpolymj.2015.04.004

Li, X. L., Han, C. L., Chen, X. Y., and Shi, C. W. (2010). "Preparation and performance of straw based activated carbon for supercapacitor in non-aqueous electrolytes," *Microporous and Mesoporous Materials* 131(1-3), 303-309. DOI: 10.1016/j.micromeso.2010.01.007

Liao, C. P., Wu, C. Z., and Yan, Y. J. (2007). "The characteristics of inorganic elements in ashes from a 1 MW CFB biomass gasification power generation plant," *Fuel Processing Technology* 88(2), 149-156. DOI: 10.1016/j.fuproc.2005.06.008

Liao, S. H., Pan, B., Li, H., Zhang, D., and Xing, B. S. (2014). "Detecting free radicals in biochars and determining their ability to inhibit the germination and growth of corn, wheat and rice seedlings," *Environmental Science & Technology* 48(15), 8581-8587. DOI: 10.1021/es404250a

Liu, X. W., Xu, M. H., Si, J. P., Gu, Y., Xiong, C., and Yao, H. (2012). "Effect of sodium on the structure and reactivity of the chars formed under N_2 and CO_2 atmospheres," *Energy & Fuels* 26(1), 185-192. DOI: 10.1021/ef2011244

Liu, Q., Wang, S. R., Zheng, Y., Luo, Z. Y., and Cen, K. F. (2008). "Mechanism study of wood lignin pyrolysis by using TG–FTIR analysis," *Journal of Analytical and Applied Pyrolysis* 82(1), 170-177. DOI: 10.1016/j.jaap.2008.03.007

Martinez, J. D., Veses, A., Mastral, A. M., Murillo, R., Navarro, M. V., Puy, N., Artigues, A., Bartroli, J., and Garcia, T. (2014). "Co-pyrolysis of biomass with waste tyres: Upgrading of liquid bio-fuel," *Fuel Processing Technology* 119, 263-271. DOI: 10.1016/j.fuproc.2013.11.015

McDonald-Wharry, J., Manley-Harris, M., and Pickering, K. (2013). "Carbonisation of biomass-derived chars and the thermal reduction of a graphene oxide sample studied using Raman spectroscopy," *Carbon* 59, 383-405. DOI: 10.1016/j.carbon.2013.03.033

Mohan, D., Kumar, H., Sarswat, A., Alexandre-Franco, M., and Pittman, C. U. (2014). "Cadmium and lead remediation using magnetic oak wood and oak bark fast pyrolysis bio-chars," *Chemical Engineering Journal* 236, 513-528. DOI: 10.1016/j.cej.2013.09.057

Mushrif, S. H., Rey, A. D., and Tekinalp, H. (2008). "Effect of metal salt on the pore structure evolution of pitch-based activated carbon microfibers," *Industrial & Engineering Chemistry Research* 47, 3883-3890. DOI: 10.1021/ie0712784

Onal, E., Uzun, B. B., and Putun, A. E. (2014). "Bio-oil production via co-pyrolysis of almond shell as biomass and high density polyethylene," *Energy Conversion & Management* 78, 704-710. DOI: 10.1016/j.enconman.2013.11.022

Peng, C., Yan, X. B., Wang, R. T., Lang, J. W., Ou, Y. J., and Xue, Q. J. (2013). "Promising activated carbons derived from waste tea-leaves and their application in high performance supercapacitors electrodes," *Electrochimica Acta* 87, 401-408. DOI: 10.1016/j.electacta.2012.09.082

Pinto, P. C. R., Oliveria, C., Costa, C. A., Gaspar, A., Faria, T., Ataide, J., and Rodrigues, A. E. (2015). "Kraft delignification of energy crops in view of pulp production and lignin valorization," *Industrial Crops & Products* 71, 153-162. DOI: 10.1016/j.indcrop.2015.03.069

Shadangi, K. P., and Mohanty, K. (2015). "Co-pyrolysis of Karanja and Niger seeds with waste polystyrene to produce liquid fuel," *Fuel* 153, 492-498. DOI: 10.1016/j.fuel.2015.03.017

Sharma, R. K., Wooten, J. B., Baliga, V. L., Lin, X. H., Chan, W. G., and Hajaligol, M. R. (2002). "Characterization of chars from pyrolysis of lignin," *Fuel* 83, 1469-1482. DOI: 10.1016/j.fuel.2003.11.015

Steinbeiss, S., and Gleixner, G. (2009). "Effect of biochar amendment on soil carbon balance and soil microbial activity," *Soil Biology & Biochemistry* 41(6), 1301-1310. DOI: 10.1016/j.soilbio.2009.03.016

Suelves, I., Lazaro, M. J., and Moliner, R. (2002). "Synergetic effects in the co-pyrolysis of samca coal and a model aliphatic compound studied by analytical pyrolysis," *Journal of Analytical & Applied Pyrolysis* 65(2), 197-206. DOI: 10.1016/S0165-2370(01)00194-2

Sun, H., Hockaday, W. C., Masiello, C. A., and Zygourakis, K. (2012). "Multiple controls on the chemical and physical structure of biochars," *Industrial & Engineering Chemistry Research* 51(9), 3587-3597. DOI: 10.1021/ie201309r

Sutton, D., Kelleher, B., and Ross, J. R. H. (2001). "Review of literature on catalysts for biomass gasification," *Fuel Processing Technology* 73(3), 155-173. DOI: 10.1016/S0378-3820(01)00208-9

Ucar, S., and Karagoz, S. (2014). "Co-pyrolysis of pine nut shells with scrap tires," *Fuel* 137, 85-93. DOI: 10.1016/j.fuel.2014.07.082

Veksha, A., Zaman, W., Layzell, D. B., and Hill, J. M. (2014). "Enhancing biochar yield by co-pyrolysis of bio-oil with biomass: Impacts of potassium hydroxide addition and air pretreatment prior to co-pyrolysis," *Bioresource Technology* 171, 88-94. DOI: 10.1016/j.biortech.2014.08.040

Wang, Q., Yan, J., Wang, Y. B., Wei, T., Zhang, M. L., Jing, X. Y., and Fan, Z. J. (2014). "Three-dimensional flower-like and hierarchical porous carbon materials as high-rate performance electrodes for supercapacitors," *Carbon* 67, 119-127. DOI: 10.1016/j.carbon.2013.09.070

Yu, J. S., Zhao, Y. C., and Li, Y. D. (2014). "Utilization of corn cob biochar in a direct carbon fuel cell," *Journal of Power Sources* 270, 312-317. DOI: 10.1016/j.jpowsour.2014.07.125

Zhang, J., Yu, L. X., Wang, Z. C., Tian, Y. M., Qu, Y. N., Wang, Y., Li, J. J., and Liu, H. Q. (2011). "Spherical microporous/mesoporous activated carbon from pulping black liquor," *Journal of Chemical Technology & Biotechnology* 86(9), 1177-1183. DOI: 10.1002/jctb.2627

Zhang, S., Min, Z. H., Tay, H. L., Asadullah, M., and Li, C. Z. (2011). "Effects of volatile-char interactions on the evolution of char structure during the gasification of Victorian brown coal in steam," *Fuel* 90(4), 1529-1535. DOI: 10.1016/j.fuel.2010.11.010

Zhou, X. Y., Zheng, F., Lv, C. L., Tang, L. J., Wei, K. C., Liu, X. Y., Du, G. B., Yong, Q., and Xue, G. (2013). "Properties of formaldehyde-free environmentally friendly lignocellulosic composites made from poplar fibres and oxygen-plasma-treated enzymatic hydrolysis lignin," *Composites Part B: Engineering* 53, 369-375. DOI: 10.1016/j.compositesb.2013.05.037

Article submitted: December 24, 2015; Peer review completed: February 27, 2016; Revised version received and accepted: March 1, 2016; Published: March 14, 2016.
DOI: 10.15376/biores.11.2.3923-3936